

Influence of micellar size on the structure of surfactant-DNA complexesA. V. Radhakrishnan¹,* S. Madhukar,[†] A. Chowdhury¹, and V. A. Raghunathan[‡]
Raman Research Institute, Bangalore 560 080, India (Received 13 April 2022; accepted 5 June 2022; published 24 June 2022)

We have studied the structure of complexes of the cationic surfactant dodecyltrimethylammonium bromide (DTAB) with DNA as a function of surfactant to DNA base molar ratio (R) and salt concentration. Small-angle x-ray scattering data show the formation of nematic gels at lower and higher salt concentrations, irrespective of the value of R . Two crystalline phases are observed over intermediate salt concentrations; a square (S) phase for $R > 3$ and a hexagonal (H_S) phase for lower R . Electron density maps of these phases show intercalated structures, with DTAB micelles sandwiched between long DNA strands. The composition of these complexes, estimated using elemental analysis, indicates that the micelles are not very long, and they occupy only about half of the interstitial volume between the DNA strands. This phase behavior is strikingly different from that of complexes of DNA with longer chain surfactants cetyltrimethylammonium bromide (CTAB) and tetradecyltrimethylammonium bromide (TTAB), which show only a hexagonal (H) phase over similar ranges of R and salt concentration, the H_S structure observed in the present study being a $\sqrt{3} \times \sqrt{3}$ superlattice of the H structure. Madelung energies of the S and H structures, calculated from the electrostatic interaction between their cylindrical constituents, suggest that the former is preferred in DTAB-DNA complexes due to the smaller micellar radius of DTAB. The propensity of DTAB to form short micelles seems also to favor the H_S phase at lower R . These results illustrate the important role of micellar size in determining the structure of these two-dimensional macro-ion crystals.

DOI: [10.1103/PhysRevE.105.064504](https://doi.org/10.1103/PhysRevE.105.064504)**I. INTRODUCTION**

Oppositely charged polyelectrolytes form complexes in aqueous solutions, driven mainly by the increase in the entropy of the counterions, which are released on complexation [1]. These polyelectrolyte complexes exhibit a wide range of structures, from disordered gels to ordered liquid crystalline phases, and they have been the subject of many studies [2,3]. Amphiphile-polyelectrolyte complexes form a special class of these systems, where one of the species is a self-assembled macro-ion, which can be either a bilayer or a micelle [4]. Complexes of DNA with bilayer-forming cationic lipids have been widely studied, motivated by their potential application in gene therapy [5–9]. These complexes have been shown to exhibit either a lamellar structure, with the DNA strands sandwiched between the bilayers, or an inverted hexagonal structure, where the DNA chains are confined to the cores of inverted cylindrical micelles. Complexes of DNA with micelle-forming cationic surfactants have also been the subject of some investigations [10–14]. Alkyltrimethylammonium bromide surfactants have been the most commonly used surfactants for these studies. Detailed structural inves-

tigations have been carried out on cetyltrimethylammonium bromide (CTAB)-DNA complexes [11,12]. They are found to have a close-packed two-dimensional hexagonal structure, where each DNA is surrounded by three cylindrical CTAB micelles and each micelle is surrounded by six DNA. The same structure is observed in complexes of DNA with tetradecyltrimethylammonium bromide (TTAB) [15]. Replacing the bromine counterion with tosylate has a pronounced effect on the structure of the complex, with cetyltrimethylammonium tosylate (CTAT)-DNA complexes showing square (S) and superhexagonal (H_S) structures, in addition to hexagonal (H) [14]. Structures of CTAT-DNA complexes have been probed as a function of the surfactant to DNA base molar ratio (R) and the surfactant concentration (C) in the solution. The S phase is observed at higher values of R over a wide range of C . The H phase occurs at lower values of R and C , whereas the H_S phase forms at lower values of R , but at higher C . Electron density maps calculated from scattering data show that the H_S structure is a $\sqrt{3} \times \sqrt{3}$ superlattice of the H structure. Formation of the S phase in this system has been attributed to the stronger binding of the tosylate counterion to the surfactant micelles, compared to the bromine counterion, and formation of the H_S phase has been attributed to the tendency of CTAT to self-assemble into very long wormlike micelles [14].

In this study, we probe the structure of complexes of high molecular weight DNA with DTAB, which is analogous to CTAB and TTAB, but with a shorter 12-carbon chain. A partial phase diagram showing the different structures exhibited by these complexes has been determined from small-angle x-ray scattering (SAXS) data, over a range of R and NaCl

*Present address: Universität Bayreuth, Experimental Physics I, Universitätsstraße 30, 95447 Bayreuth, Germany.

†Present address: Advanced Characterization Technology Laboratory, Dr. Reddy's Laboratories Ltd., Bachupally, Hyderabad 500090, India.

‡varaghu@rri.res.in

concentration in the solution. These complexes form a nematic phase at low and high values of [NaCl], characterized by long-range orientational order and short-range positional order. Two-dimensional crystalline structures are observed over intermediate values of [NaCl]; a square (S) phase at $R > 3$ and a superhexagonal (H_S) phase at lower R . From the experimentally estimated compositions of these complexes, it can be concluded that the DTAB micelles occupy only about half the interstitial volume between the DNA. This phase behavior is in striking contrast to that of CTAB-DNA and TTAB-DNA complexes, which exhibit only a hexagonal phase irrespective of the value of R . The structure of the S phase is similar to that observed in CTAT-DNA complexes. However, estimation of the electrostatic energy of the hexagonal and square phases indicates that the stability of the S phase in DTAB-DNA complexes is due to the lower micellar radius of DTAB compared to CTAB. The H_S phase of DTAB-DNA complexes does not transform into the H phase on application of an osmotic pressure, as was observed in the case of CTAT-DNA complexes [16]. This suggests that the H_S phase of DTAB-DNA complexes might have a different structure, compared to that of the same phase observed in CTAT-DNA complexes. However, with the available scattering data, we are unable to unambiguously elucidate the structure of this phase in the present system.

II. EXPERIMENT

DTAB, the sodium salt of calf thymus DNA, NaCl, and polyvinylpyrrolidone of molecular weight 10 000 (PVP10000), were obtained from Sigma-Aldrich. Complexes were prepared by adding appropriate amounts of DNA to an aqueous solution of the surfactant and NaCl, to obtain the desired value of the surfactant to DNA base molar ratio, R . We have also prepared some samples by mixing a micellar solution with a DNA solution. Identical structures are obtained in both cases. The size of the crystallites is generally larger in the first protocol, giving rise to sharper peaks in the SAXS pattern. Hence it was used in all the studies reported here. In one set of experiments, the surfactant concentration in the solution was held at 20 mM, and NaCl concentration was varied from 0 to 500 mM for R ranging from 0.5 to 5. In a second set of experiments, the surfactant concentration was varied from 50 to 400 mM in the absence of NaCl for the same range of R . The complexes form a gel-like precipitate suspended in the supernatant, which contains either excess DNA or surfactant, depending on the value of R chosen. Hence the composition of the complex, R_c , is in general different from the global composition of the solution, R . The supernatant also contains the Na^+ and Br^- counterions released from DNA and surfactant, respectively, in addition to the added NaCl. The samples were equilibrated for about a week. For SAXS studies, the complex along with some of the supernatant was taken in 1 mm glass capillaries, which were flame-sealed to avoid any loss of water. Data were collected over a range of the magnitude of the scattering vector (q) from 0.01 to 5.0 nm^{-1} , using a Hecus S3-Micro system, fitted with a one-dimensional position-sensitive detector. Typical exposure time was 30 min, and error in the measurement of peak positions was ± 0.02 nm. All data were collected at 30 °C. We have collected data from

the same sample multiple times and have not observed any changes in the SAXS pattern. Hence any degradation caused by exposure to the x-ray beam is negligible. We also checked SAXS patterns of some of the samples about 3 weeks after the initial equilibration period, and we did not observe any changes. This strongly suggests that the observed structures are in equilibrium and are not kinetically trapped.

For the osmotic pressure experiments, samples were prepared at selected DTAB and DNA concentrations, as described above, and were equilibrated for about a week. Appropriate amounts of PVP10000 were added to the supernatant in order to get the desired final polymer concentration in the aqueous medium. The polymer solution forms a separate phase coexisting with the complex and hence applies an osmotic pressure on it. This method does not require the use of a semipermeable membrane, and it has been employed in probing many soft matter systems [17,18]. Polymer concentration in the solution was varied from 0 to 20 wt. %, covering a range of osmotic pressure from 0 to 7×10^5 Pa [19]. The samples were then sealed and left to equilibrate for 10 more days. For SAXS studies, the complex along with some supernatant was taken in glass capillaries and flame-sealed.

Elemental analysis of the complexes was conducted using a CHNS elemental analyzer (vario MICRO cube, Elementar), which gives the relative amounts of C, H, and N in the material to an accuracy of 0.3%. Complexes were prepared at chosen compositions, and the entire complex was transferred into tin boats after equilibration. Care was taken to minimize the amount of the supernatant taken along with the complex. The samples were then dried thoroughly by being placed in an evacuated desiccator for 3 days. Complete drying was ensured by repeated weighing in an ultramicrogram balance (Sartorius). The samples were then removed and crimped immediately to avoid rehydration.

Elemental analysis gives the total carbon and nitrogen content (weights) of the complex. The weights of these elements obtained from the experiment are converted into moles using the appropriate atomic weights. The total number of carbon and nitrogen atoms in the complex can be expressed as $C_t = n_s C_s + n_b C_b$ and $N_t = n_s N_s + n_b N_b$, where C_s , C_b , N_s , and N_b are the number of carbon and nitrogen atoms in each surfactant and DNA base, respectively, and n_s and n_b are the number of surfactant molecules and DNA bases in the sample. For the present system, $C_s = 15$, $C_b = 9.8$, $N_s = 1$, and $N_b = 3.7$. Average values for a DNA base were obtained by taking the ratio of adenine—thymine and guanine—cytosine base pairs to be 58.1% and 41.9%, respectively [20]. Recasting the above equations, we get $C_t/N_t = (C_s R_c + C_b)/(R_c + N_b)$. Thus $R_c (=n_s/n_b)$ can be estimated from the values of C_t and N_t obtained from the experiment.

III. RESULTS

A. SAXS

SAXS data were collected for R ranging from 0.5 to 5.0 and for [NaCl] varying from 0 to 500 mM. SAXS patterns obtained at $R = 5.0$ for different values of [NaCl] are presented in Fig. 1. In the absence of NaCl, the SAXS pattern shows only a broad peak, indicating the absence of long-range

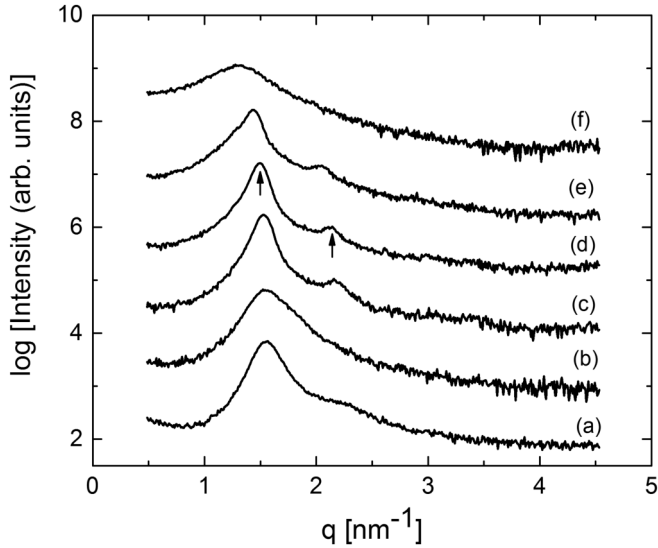


FIG. 1. SAXS patterns of DTAB-DNA complexes at $R = 5.0$ for $[\text{NaCl}] = 0$ mM (a), 100 mM (b), 200 mM (c), 300 mM (d), 400 mM (e), and 500 mM (f). Arrows indicate the positions of the (1 0) and (1 1) peaks from a square lattice.

positional order in the system. Polarizing microscopy images show that the complex is birefringent and hence is characterized by long-range orientational order (Fig. 2). We refer to this as the Nematic Gel I. This structure is obtained up to $[\text{NaCl}] \sim 200$ mM. As $[\text{NaCl}]$ is increased further, peaks in the diffraction pattern become sharper and more distinct. These patterns show up to four peaks, with their q 's in the ratio $1:\sqrt{2}:2:\sqrt{5}$, and they can be indexed on a two-dimensional square lattice, with the lattice parameter $a_S \approx 4.5$ nm. We label this the square (S) phase. Peaks in the diffraction pattern become broad with a further increase in $[\text{NaCl}]$. These complexes are birefringent, and we label this structure as the Nematic Gel II (Fig. 2). Complexes do not form on increasing $[\text{NaCl}]$ beyond 600 mM, and a uniform solution is obtained.

SAXS patterns obtained at $R = 0.5$ for different values of $[\text{NaCl}]$ are given in Fig. 3. The behavior at $R = 0.5$ is very similar to that at $R = 5.0$, with the appearance of SAXS patterns with sharp peaks only over an intermediate range of $[\text{NaCl}]$. Both at higher and lower $[\text{NaCl}]$ the birefringent complexes give only a very broad peak in their SAXS patterns. However, the ordered structure found at $R = 0.5$ corresponds to a two-dimensional hexagonal lattice and not a square lattice. Moreover, in all these patterns, the (1 0) peak is always absent and only higher-order peaks with their q 's in the ratio $\sqrt{3}:2:\sqrt{7}:3:\sqrt{12}$ are observed. The lattice parameter of this phase is $a_H \approx 9.0$ nm, and we refer to this as the superhexagonal (H_S) phase.

A partial phase diagram of the system, as a function of R and $[\text{NaCl}]$, deduced from the SAXS data is presented in Fig. 4(a). Nematic phases are found at lower and higher $[\text{NaCl}]$ for all values of R . Over intermediate values of $[\text{NaCl}]$, the S phase is observed for $R > 3$, whereas the H_S structure is observed at lower R . Figure 4(b) shows the phase behavior as a function of R and surfactant concentration in the absence of salt. Here the nematic phase is observed at lower DTAB

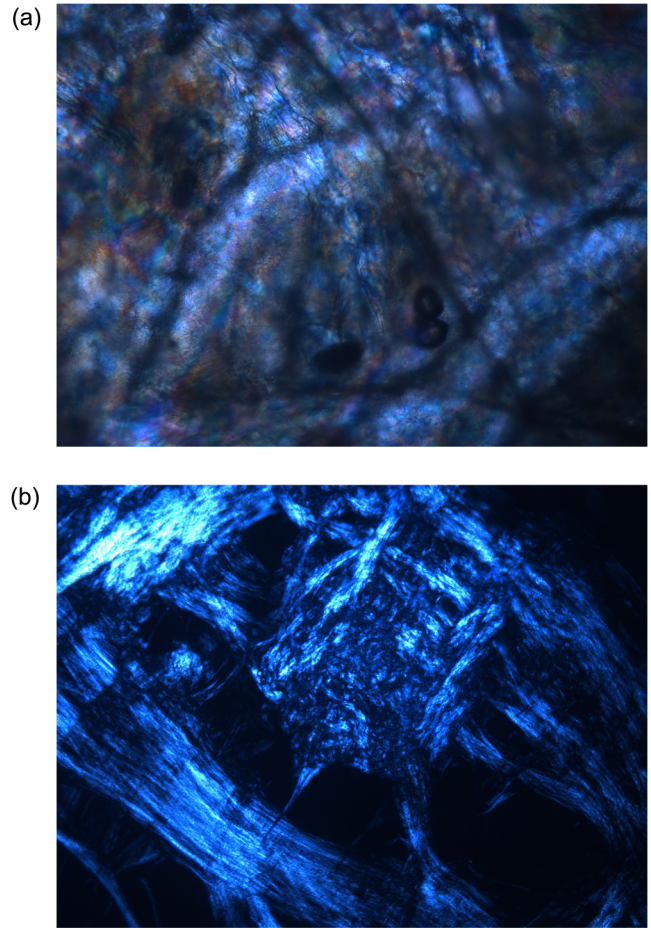


FIG. 2. Polarizing optical microscopy images of Nematic Gel I (a) and Nematic Gel II (b) complexes under crossed polarizers at $R = 1$ and $[\text{NaCl}] = 0$ and 500 mM, respectively.

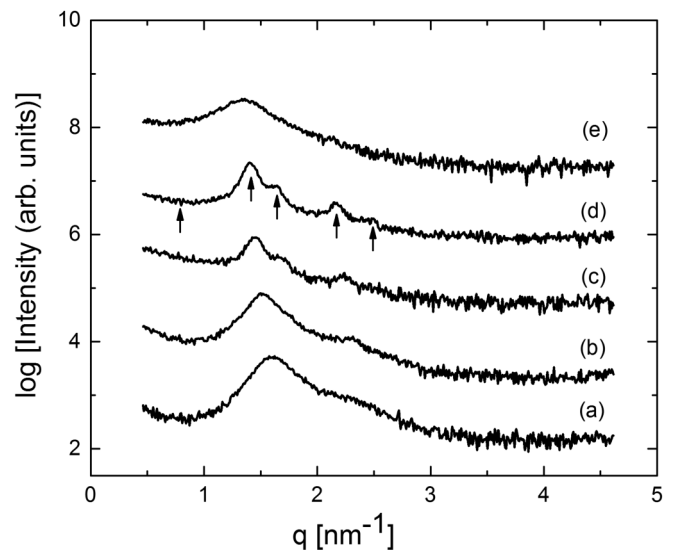


FIG. 3. SAXS patterns of DTAB-DNA complexes at $R = 0.5$ for $[\text{NaCl}] = 0$ mM (a), 100 mM (b), 200 mM (c), 300 mM (d), and 400 mM (e). Arrows indicate positions of the (1 0), (1 1), (2 0), (2 1), and (3 0) peaks from a hexagonal lattice. Note the absence of the (1 0) peak.

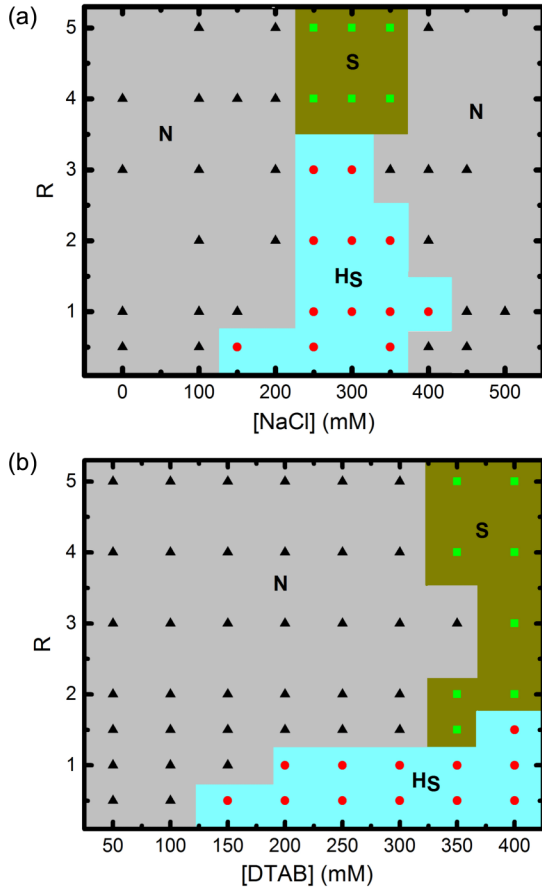


FIG. 4. Partial phase diagrams of DTAB-DNA complexes determined from SAXS and polarizing microscopy data, as a function of R and NaCl concentration (a) and as a function of R and DTAB concentration (b). N , nematic; S , square; and H_S , superhexagonal. $[DTAB] = 20$ mM in (a).

concentrations, irrespective of the value of R . The H_S phase appears on increasing $[DTAB]$ to 150 mM for $R \leq 1$, whereas the S phase occurs for $[DTAB] \geq 350$ mM for $R \geq 2$.

B. Elemental analysis

Results of elemental analysis of DTAB-DNA complexes at different values R and at $[NaCl] = 300$ mM are given in Table I. Here R is the surfactant to DNA base molar ratio in the

TABLE I. Elemental analysis data of DTAB-DNA complexes at $[NaCl] = 300$ mM. R is the DTAB to DNA base molar ratio in the whole solution, and R_c is its value in the complex.

R	N (wt%)	C (wt%)	R_c
0.5	4.89	18.89	0.66
1.0	8.50	34.35	0.74
2.0	8.73	37.30	0.86
2.5	9.27	45.23	1.21
3.0	8.38	41.93	1.29
3.5	8.23	41.75	1.33
4.0	8.68	42.85	1.31
5.0	9.66	49.22	1.35

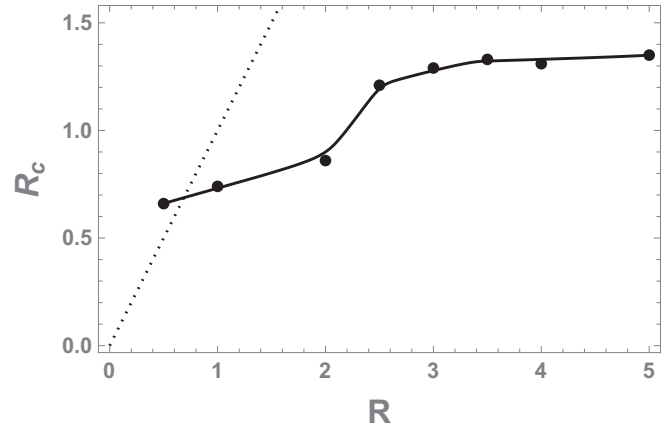


FIG. 5. Variation of R_c with R obtained from elemental analysis of DTAB-DNA complexes at $[NaCl] = 300$ mM. The dashed line corresponds to $R_c = R$.

whole solution, and R_c is its value in the complex. Variation of R_c with R obtained from these data is shown in Fig. 5. At $R = 0.5$, R_c is slightly higher, indicating that the supernatant contains excess DNA. For $R > 1$, R_c is less than R and the supernatant contains excess surfactant. R_c increases gradually with R initially and exhibits a small jump at $R \sim 2.5$, beyond which it saturates.

C. Madelung energy

CTAB-DNA complexes exhibit only the hexagonal (H) structure irrespective of the value of R . In contrast, this structure is absent in DTAB-DNA complexes, and the S structure is observed for $R > 3$. To gain a qualitative understanding of the relative stability of the S and H structures, we have estimated their electrostatic energy. Assuming the micelles to be infinitely long, the electrostatic energy of these two-dimensional macro-ion crystals can be estimated using the pair interaction potential per unit length between two dissimilar parallel cylinders, separated by a distance r , given by [21]

$$V(r) = 2(v_1 v_2 / \epsilon) K_0(\kappa r), \tag{1}$$

where $v_i = 2\pi\sigma_i / \kappa K_1(\kappa a_i)$, σ_i is the surface charge density of the cylinder of radius a_i ($i = 1, 2$), and κ is the inverse Debye length. K_0 and K_1 are Bessel functions of the second kind of order 0 and 1, respectively. The energy U of the macro-ion crystal per unit cell can be obtained by summing the interactions of each particle in the unit cell with all other particles in the system, analogous to the calculation of the Madelung energy of ionic crystals [22–25],

$$U = \frac{1}{2} \sum V_{mm}(r) + \sum V_{md}(r) + \frac{1}{2} \sum V_{dd}(r). \tag{2}$$

The three terms in the above equation correspond to the micelle-micelle, micelle-DNA, and DNA-DNA interactions, respectively.

The surface charge density of the micelle is estimated to be 1.56 e/nm², taking the area per head group to be 0.64 nm² [26], whereas that of the DNA is estimated to be -0.75 e/nm² from its radius of 1.25 nm [5]. The energies of the

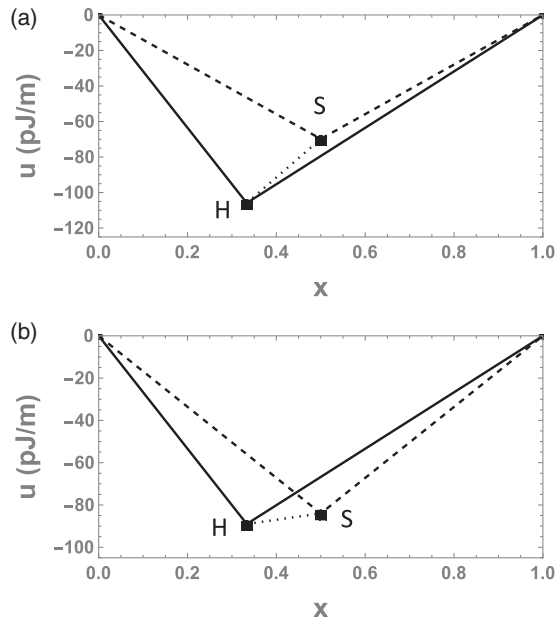


FIG. 6. Electrostatic energy per particle of the S and H structures obtained from the calculations. x is the ratio of the number of micelles to the total number of particles (DNA + micelles) in a unit cell. $x = 1/3$ for H and $x = 1/2$ for S . $x = 0$ and 1 correspond to dilute solutions of DNA and micelles, respectively. The straight line segments are Maxwell constructions joining any two of the four energy minima corresponding to the four phases in the system. The two phases coexisting at any value of x are indicated by the end points of the lowest straight line segment at that composition. $[\text{NaCl}] = 300$ mM. $r_m = 2.0$ nm (a) and $r_m = 1.5$ nm (b).

two structures have been calculated by summing over these interactions using the Sum routine from MATHEMATICA [27]. Since the electrostatic interactions are screened by salt, the summation converges rapidly over a few unit cells.

The energy per particle, $u = U/n$, n being the number of particles within a unit cell, of the H and S structures obtained from the calculations is given in Fig. 6 for $r_m = 2.0$ and 1.5 nm. Here x is the micelle/(DNA + micelle) fraction in the structure, values of x for H and S being 1/3 and 1/2, respectively. The points $x = 0$ and 1 represent dilute solutions of DNA and micelles, respectively, whose electrostatic energy is assumed to vanish. The coexistence of different structures can be inferred from the slopes of the straight lines joining the points representing their energies, a procedure analogous to the well-known Maxwell construction [25]. H is found to be the only stable structure for $r_m = 2.0$ nm. It coexists with a dilute DNA solution between $x = 0$ and 1/3, and with a dilute micellar solution at higher values of x . On decreasing r_m to 1.5 nm S also becomes stable, leading to its coexistence with H between $x = 1/3$ and 1/2, and with a dilute micellar solution between $x = 1/2$ and 1.

The negative contribution to u from micelle-DNA interaction is comparable in the two structures at a given value of r_m . The positive contribution from micelle-micelle interaction is higher in S , due to the lower intermicellar separation in this structure. For similar reasons, the positive contribution from DNA-DNA interaction is higher in H . Since the surface

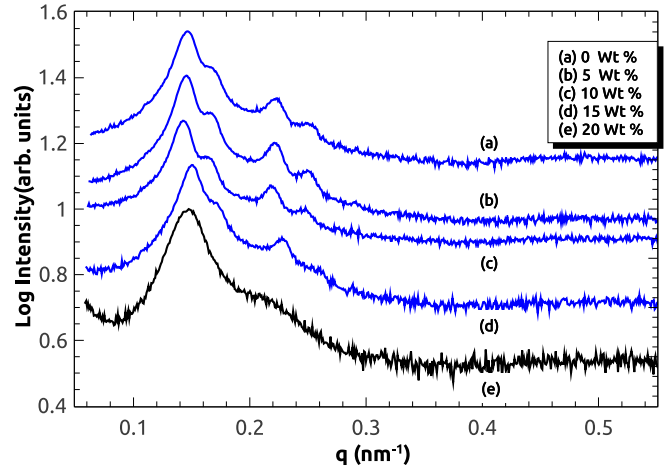


FIG. 7. SAXS patterns of DTAB-DNA complexes in the H_S phase at $R = 1.0$ for different PVP10000 concentrations in the solution.

charge density of the micelle is assumed to be fixed, its total charge increases with increasing r_m . Hence the magnitudes of the micelle-DNA and micelle-micelle interactions are higher at higher r_m . On the other hand, the DNA-DNA contributions are lower at higher r_m , since the inter-DNA separation increases with increasing r_m . At $r_m = 1.5$ nm, the two structures have comparable values of u and hence they are both stable, albeit at different compositions. On increasing r_m to 2, DNA-DNA repulsion decreases in H , whereas micelle-micelle repulsion increases in S , leading to the disappearance of the latter from the phase diagram.

D. Effect of osmotic pressure

The H_S phase of CTAT-DNA complexes is a slightly swollen version of H , and it can be transformed into the latter by the application of a moderate osmotic pressure of $\sim 1.0 \times 10^5$ Pa [16]. To check if a similar transformation takes place in DTAB-DNA complexes, we have studied the effect of osmotic pressure on the H_S phase of DTAB-DNA complexes. SAXS patterns of the complexes at different PVP10000 concentrations are given in Fig. 7. The lattice parameter decreases from 8.7 to 8.5 nm as the PVP10000 concentration in the solution is increased from 0 to 15 wt. %, which corresponds to an osmotic pressure of 5.4×10^5 Pa. But no transition to the H phase is observed. At a polymer concentration of 20 wt. % (7.0×10^5 Pa), the complex becomes disordered, giving only a broad peak in the SAXS pattern; a similar disordering of CTAT-DNA complexes is observed at a comparable value of the osmotic pressure [16]. Similar results have been obtained using PEG8000 to apply the osmotic pressure, instead of PVP10000.

E. Effect of micellar length

Based on the Madelung energy calculations presented earlier, we would have expected to observe the H phase in DTAB-DNA complexes at lower values of R , as in the case of CTAB-DNA complexes, and not the H_S phase. One major difference between these two surfactants is the tendency

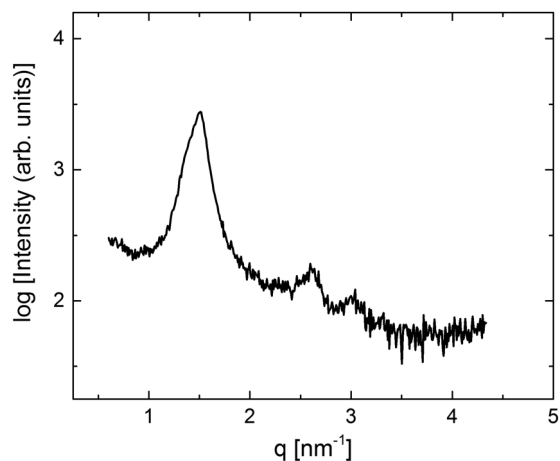


FIG. 8. SAXS pattern showing the formation of the H phase in DTAB-DNA complexes in the presence of hexanol. The three peaks can be indexed as $(1\ 0)$, $(1\ 1)$, and $(2\ 0)$. Hexanol to surfactant molar ratio in the solution is 1.0, $R = 0.5$, and $[\text{DTAB}] = 50\ \text{mM}$.

of CTAB to form cylindrical micelles, compared to small ellipsoidal micelles in the case of DTAB [28]. To probe if this

difference is responsible for the occurrence of the two different structures, we have studied the influence of hexanol on the phase behavior of DTAB-DNA complexes, since hexanol is known to induce the formation of cylindrical micelles [29]. SAXS patterns of the complexes at a hexanol to surfactant molar ratio in the solution, $\beta = 1$, are shown in Fig. 8. It has three peaks, with their q 's in the ratio $1:\sqrt{3}:2$, which can be indexed on a two-dimensional hexagonal lattice with $a = 4.7\ \text{nm}$. Thus the elongation of the micelles drives an $H_S \rightarrow H$ transition of the complex.

F. Electron density maps

Electron density maps $[\rho(\vec{r})]$ of the different structures observed in this study have been determined from the SAXS data, using the relation $\rho(\vec{r}) = \sum_{hk} |F_{hk}| \phi_{hk} \cos(\vec{q}_{hk} \cdot \vec{r})$, where $|F_{hk}|$, ϕ_{hk} and \vec{q}_{hk} are the amplitude, phase, and scattering vector, respectively, of the (h, k) reflection. Assuming the structure to have a center of symmetry, ϕ_{hk} is taken to be either $+1$ or -1 . $\rho(\vec{r})$ is computed by trying out all phase combinations and picking out the most suitable map(s) consistent with a close-packed structure of DNA and micelles. Electron density maps, so determined, are shown in Fig. 9.

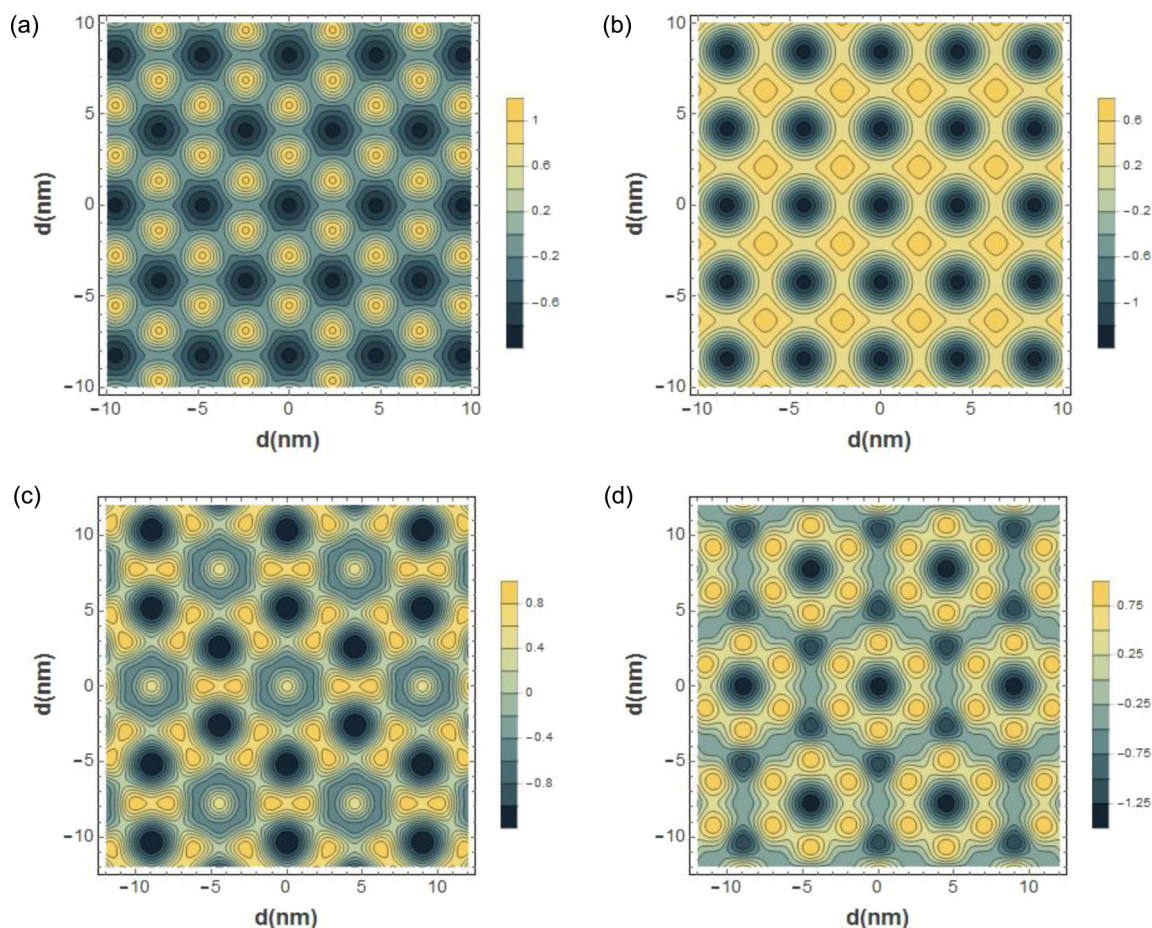


FIG. 9. Electron density maps of the H (a), S (b), and H_S phases (c),(d) observed in the present study, determined from the SAXS data. Two possible structure of the H_S phase are shown, which are obtained for different sets of phases of the observed reflections. These maps correspond to the electron density of the complexes projected on the plane of the lattice, which is normal to the DNA axis. The low electron density regions correspond to the hydrocarbon cores of the micelles, and the high electron density regions correspond to DNA.

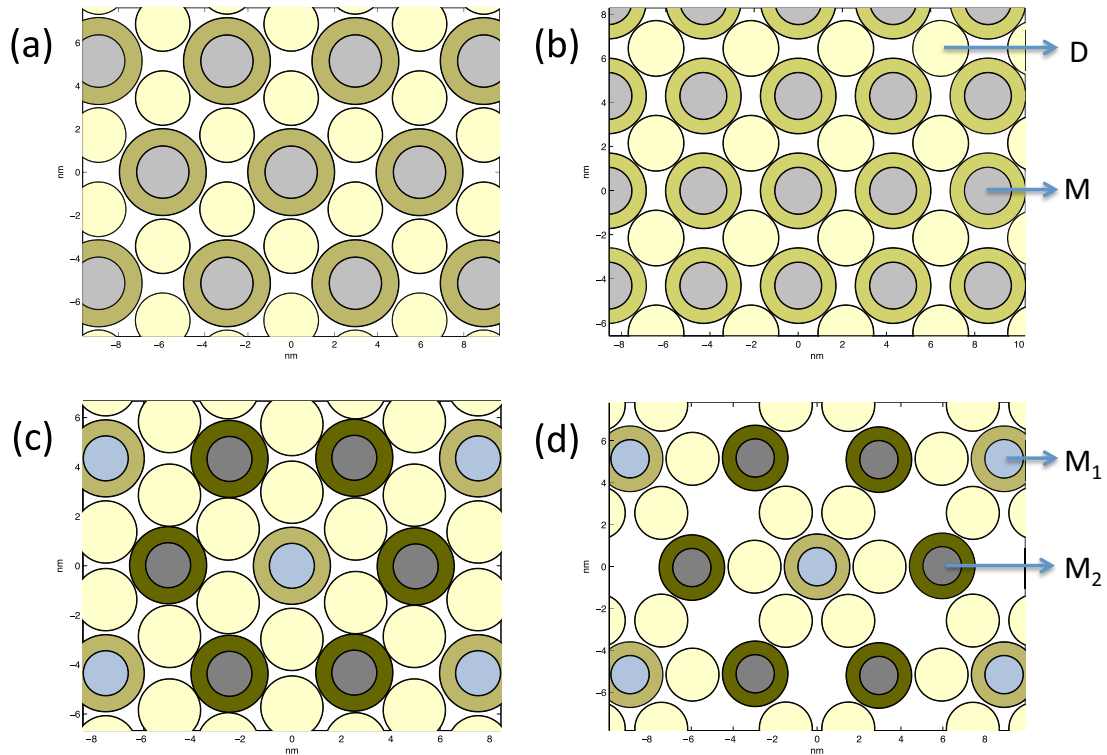


FIG. 10. Schematics of the structures of the H (a), S (b), and H_S (c),(d) phases observed in the present study, deduced from the electron density maps given in Fig. 9. The cross-section of DNA is represented by the smaller uniform disk (D) and that of the micelle (M) is shown as a central disk representing the hydrocarbon core, surrounded by an annular head-group region. Note the presence of two types of micelles (M_1 and M_2) in the H_S structure.

The schematics of various structures suggested by these maps are given in Fig. 10.

IV. DISCUSSION

SAXS data and polarizing optical microscopy observations show the formation of a nematic phase at low DTAB concentrations for all values of R . It may be noted here that the SAXS profile of the $R = 1$ complex in the absence of salt, whose microscopy texture is presented in Fig. 2, is almost identical to those of the $R = 0.5$ and 5 samples under similar conditions (Fig. 3), indicating that they all have the same structure. DTAB is known to form small ellipsoidal micelles at lower concentrations [28]. The lack of long-range translational order in these complexes most probably results from these micelles taking different orientations between the DNA strands. Increasing the salt or surfactant concentration results in elongated micelles, which can pack more uniformly between the DNA [28]. As a consequence, two-dimensional crystalline structures characterized by long-range translational order are formed under these conditions. A nematic phase is again observed at high NaCl concentrations. This results from the gradual swelling of the complex due to the screening of electrostatic interactions by increasing salt concentration in the solution, which destroys long-range translational order resulting in the orientationally ordered nematic phase. With a further increase in the salt concentration, long-range orientational order is also lost, and complexation is completely

prevented. As a result, a uniform solution is obtained for $[\text{NaCl}] > 600$ mM.

The phase diagrams show the formation of the S and H_S phases in DTAB-DNA complexes, in contrast to CTAB-DNA and TTAB-DNA complexes, where only the H phase is seen. Elemental analysis studies indicate that the composition of the complex is $R_c \sim 1$ in both phases (Fig. 5). Hence concentrations of Na^+ and Br^- counterions in the solution can be expected to be comparable to the DTAB concentration. Therefore, it is understandable that the S and H_S phases appear at comparable values of $[\text{NaCl}]$ and $[\text{DTAB}]$ in the two phase diagrams. However, there are slight differences in the positions of the phase boundaries in Figs. 4(a) and 4(b). In the former case, the concentration of Br^- is around 50 mM and that of Cl^- increases with increasing NaCl in the solution. In the latter case, Cl^- is absent and Br^- concentration increases with DTAB concentration. Therefore, it is possible that the differences in the locations of the phase boundaries are due to the presence of different dominant counterions in the two solutions. The small jump in R_c observed at $R \sim 2.5$ coincides with the $H_S \rightarrow S$ transition observed in SAXS studies, and it implies an abrupt increase in the surfactant content of the complex on forming the S phase. R_c can be estimated from the proposed structures of the complexes, assuming that the micelles are infinitely long [16]. With this assumption, the micelle to DNA stoichiometry is 1:1 and 1:2 in the S and H_S structures, respectively (Fig. 10). Taking the DTAB micellar radius $r_m = 1.75$ nm, R_c turns out to be 2.8 and 1.4 in the S and H_S phases, respectively. Values obtained from elemental

analysis data are almost half the estimated values in the two phases. This indicates that the DTAB micelles in these complexes are not very long and occupy only about half of the interstitial volume between the DNA strands.

The structure of the S phase of the present system, indicated by Fig. 9(b), is identical to that of the S phase of CTAT-DNA complexes, which has been established from a detailed analysis of the scattering data [14]. The tosylate counterion of CTAT has a hydrophobic moiety and hence it binds much more strongly to the micelle compared to the Br^- counterion of CTAB and DTAB. The formation of the S phase of CTAT-DNA complexes, which also occurs at higher values of R , has been attributed to this property of the counterion. But the counterion cannot be implicated in the formation of the S phase in DTAB-DNA complexes, since this phase is absent in complexes of DNA with CTAB and TTAB, which have the same Br^- counterion as DTAB. The Madelung energy calculations presented above suggest that the S structure is preferred over the H structure when the micellar radius is smaller than a threshold value. Hence the stability of the S phase in DTAB-DNA complexes can be attributed to the lower radius of DTAB micelles. The composition variable x , appearing in these calculations, is related to R_c . They both describe the composition of the complex: x in terms of the number of micelles and DNA, and R_c in terms of the number of surfactant molecules and DNA bases. As discussed earlier, R_c can be estimated to be 1.4 and 2.8 in the H and S structures of DTAB-DNA complexes, respectively, assuming the micelles to be infinitely long. Hence $x = 0, 1/3, 1/2$, and 1 correspond to $R_c = 0, 1.4, 2.8$, and ∞ , respectively. We do not expect this result to change even if the micelles are taken to be of finite length, especially if the arrangement of the micelles along the direction normal to the lattice plane is assumed to be random, as found in the two-dimensional structures observed in the present study. The precise value of the micellar radius at which this transformation occurs will most probably be dependent on the micellar length. The assumption of infinitely long micelles is justifiable, as we do not attempt a quantitative comparison with the experimental data, and we are only interested in the qualitative trends.

Two kinds of electron density maps are obtained for the H_S phase, which can be interpreted in terms of intercalated packings of DNA and micelles. The unit cell in both cases corresponds to a $\sqrt{3} \times \sqrt{3}$ superlattice of the H structure. There are two nonequivalent micellar environments in both maps, creating the superlattice. Both of the unit cells contain one micelle of type-1, two micelles of type-2, and six DNA (Fig. 10). They consist of clusters made up of six DNA surrounding a central type-1 micelle that are crossed-linked by type-2 micelles. The only difference between these two structures is a relative rotation of the clusters by 30° with respect to the line joining neighboring type-1 and type-2 micelles. If we ignore the differences between the two types of micelles, these structures have a micelle to DNA stoichiometry of 1:2, the same as that in the H phase (Fig. 10). In the case of CTAT-DNA complexes, the first structure has been shown to be in better agreement with the scattering data [14]. This is a slightly swollen version of the H phase, and it can be transformed into it by the application of an osmotic pressure [16]. Such a swollen structure can be maintained in this case

as CTAT forms very long wormlike micelles. In the present case, it has not been possible to distinguish between these two structures from an analysis of the scattering data similar to that presented in Ref. [14]. Nevertheless, the fact that an osmotic pressure-driven $H_S \rightarrow H$ transition is not observed may be an indication that the second structure is the appropriate one in the present case. It is also difficult to imagine the formation of a swollen structure, as in the case of CTAT-DNA complexes, since DTAB forms much shorter micelles.

In the case of CTAT-DNA complexes, we were able to fit the observed SAXS data to two electron density models based on the two proposed structures for the H_S phase [14]. One of the models gives a better fit to the data, and values of the model parameters obtained from the best fit show that the two types of micelles have slightly different sizes and different electron densities in the head-group region. We would expect a similar situation here. In the present case, however, both of these models give comparable fits to the data, and hence we are unable to pick out a unique solution. However, both the models are consistent with differences in size and head-group electron density of the two types of micelles.

The observed effect of hexanol on DTAB-DNA complexes suggests that elongation of the micelles leads to the transformation of H_S into H . The structure of the H phase of DTAB-hexanol-DNA complexes, inferred from the scattering data, is identical to that of CTAB-DNA complexes [30]. Hence the occurrence of the H_S structure in this system is somehow related to the propensity of DTAB to self-assemble into small micelles. It is rather surprising that the H_S phase has been observed in complexes of DNA with surfactants that self-assemble into both very long and very short micelles, such as CTAT and DTAB, respectively. On the other hand, in complexes of DNA with surfactants that form intermediate rodlike micelles, such as CTAB, this phase is absent. Currently we do not know the precise factors that stabilize this phase; it is conceivable that different mechanisms are at play in the two limiting cases of micellar length.

It is possible to imagine other possible structures of the H_S phase made up of short micelles. For example, a three-dimensional structure can be considered, where the positions of neighboring micelles are staggered along the DNA axis, resulting in a centered lattice. However, in the present case all the observed reflections can be indexed accurately on a two-dimensional lattice, and hence there is no justification to invoke such a three-dimensional structure. Another possibility is a structure with orientationally disordered DNA-micelle clusters, as shown in Fig. 11. Such a structure can result from both of the H_S structures presented in Figs. 9 and 10 if there is no long-range order in the orientation of the DNA-type-1 micelle clusters with respect to the hexagonal lattice. It is conceivable that elongation of the micelles would restore orientational order of the clusters, leading to the formation of the H phase, as observed. With the limited scattering data available, we are unable to rule out these different possibilities.

V. CONCLUSIONS

We have probed the structure of DTAB-DNA complexes over a wide range of surfactant to DNA molar ratio and salt

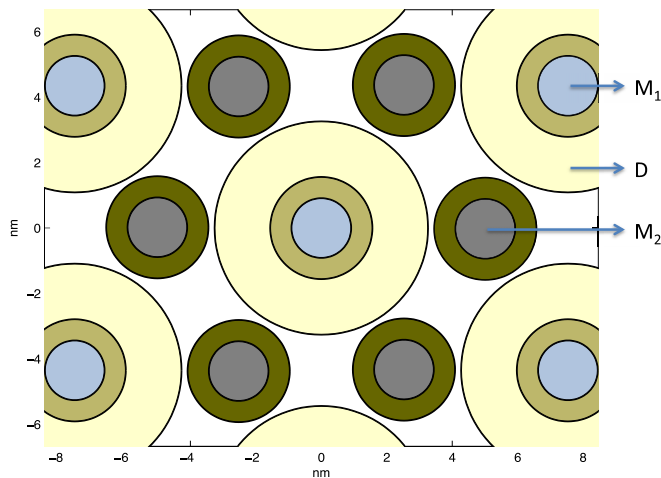


FIG. 11. Schematic of a structure of the H_5 phase consisting of orientationally disordered type-1 micelle–DNA clusters cross-linked by type-2 micelles (M_2). Due to the orientational disorder of the clusters, the DNA form an annular region (D) surrounding type-1 micelles (M_1) in the projection on the plane of the lattice.

concentration. A phase diagram of the system has been determined from the experimental data. Two crystalline phases are observed over intermediate salt concentrations: a square phase and a superhexagonal phase, respectively, at higher and lower

surfactant to DNA relative concentration. This phase behavior is very different from that of complexes of DNA with analogous but longer chain surfactants, CTAB and TTAB, which show only a hexagonal phase. Madelung energy calculations show that the stability of the square phase in DTAB–DNA complexes can be attributed to the lower micellar radius of DTAB compared to CTAB. The formation of the superhexagonal phase, on the other hand, seems to be a consequence of the tendency of DTAB to self-assemble into shorter micelles. These results demonstrate the important role played by the surfactant chain length, which determines the micellar size and shape, in the phase behavior of these two-dimensional macro-ion crystals. Complexes of DNA with alkyltrimethylammonium surfactants have been used to fabricate photonic and electroluminescent devices [31,32]. It is conceivable that a particular structure of these complexes is more suitable for a given application. Hence a better understanding of the structural polymorphism of these complexes, such as that provided by the present study, will be very useful in optimizing these materials for various applications.

ACKNOWLEDGMENTS

This work was funded by the Department of Science and Technology, Government of India. V.A.R. thanks the Indian National Science Academy for support under the Senior Scientist Program.

- [1] Z. Ou and M. Muthukumar, *J. Chem. Phys.* **124**, 154902 (2006).
- [2] C. E. Sing and S. L. Perry, *Soft Matter* **16**, 2885 (2020).
- [3] C. G. de Kruijff, F. Weinbreck, and R. de Vries, *Curr. Opin. Colloid Interface Sci.* **9**, 340 (2004).
- [4] M. Wang and Y. Wang, *Soft Matter* **10**, 7909 (2014).
- [5] J. O. Rädler, I. Koltover, T. Salditt, and C. R. Safinya, *Science* **275**, 810 (1997).
- [6] D. D. Lasic, H. Strey, M. C. A. Stuart, R. Podgornik, and P. M. Frederik, *J. Am. Chem. Soc.* **119**, 832 (1997).
- [7] I. Koltover, T. Salditt, J. O. Rädler, and C. R. Safinya, *Science* **281**, 78 (1998).
- [8] R. Bruinsma, *Eur. Phys. J. B* **4**, 75 (1998).
- [9] S. May, D. Harries, and A. Ben-Shaul, *Biophys. J.* **78**, 1681 (2000).
- [10] C. Leal, L. Wadsö, G. Olofsson, M. Miguel, and H. Wennerström, *J. Phys. Chem. B* **108**, 3044 (2004).
- [11] R. Krishnaswamy, V. A. Raghunathan, and A. K. Sood, *Phys. Rev. E* **69**, 031905 (2004).
- [12] R. Krishnaswamy, G. Pabst, M. Rappolt, V. A. Raghunathan, and A. K. Sood, *Phys. Rev. E* **73**, 031904 (2006).
- [13] C. Leal, E. Moniri, L. Pegado, and H. Wennerström, *J. Phys. Chem. B* **111**, 5999 (2007).
- [14] A. V. Radhakrishnan, S. K. Ghosh, G. Pabst, V. A. Raghunathan, and A. K. Sood, *Proc. Natl. Acad. Sci. (USA)* **109**, 6394 (2012).
- [15] M. Thomas, A. Chowdhury, A. Majhi, and V. A. Raghunathan, *Liq. Cryst.* (to be published).
- [16] S. Madhukar, A. V. Radhakrishnan, and V. A. Raghunathan, *Phys. Rev. E* **103**, 022705 (2021).
- [17] J. DeRouchey, R. R. Netz, and J. O. Rädler, *Eur. Phys. J. E* **16**, 17 (2005).
- [18] B.-S. Lu, S. P. Gupta, M. Belička, R. Podgornik, and G. Pabst, *Langmuir* **32**, 13546 (2016).
- [19] URL <https://scholars.huji.ac.il/danielharries/book/osmotic-stressdata>.
- [20] J. C. Wang, *Proc. Natl. Acad. Sci. (USA)* **76**, 200 (1979).
- [21] S. L. Brenner and V. A. Parsegian, *Biophys. J.* **14**, 327 (1974).
- [22] M. E. Leunissen, C. Christova, A.-P. Hynninen, C. P. Royall, A. I. Campbell, A. Imhof, M. Dijkstra, R. van Roij, and A. van Blaaderen, *Nature (London)* **437**, 235 (2005).
- [23] G. R. Maskaly, R. E. Garcia, W. C. Carter, and Y.-M. Chiang, *Phys. Rev. E* **73**, 011402 (2006).
- [24] G. R. Maskaly, Ph.D. thesis, Massachusetts Institute of Technology (2005).
- [25] D. van den Berg, Master's thesis, Utrecht University (2009).
- [26] F. Reiss-Husson and V. Luzzati, *J. Phys. Chem.* **68**, 3504 (1984).
- [27] Wolfram Research, Inc., Mathematica, Version 11.0 (2016).
- [28] M. Bergström and J. Skov Pedersen, *Phys. Chem. Chem. Phys.* **1**, 4437 (1999).
- [29] T. Schmutzler, T. Schindler, M. Schmiele, M.-S. Appavou, S. Lages, A. Kriele, R. Gilles, and T. Unruh, *Colloids Surf. A* **543**, 56 (2018).
- [30] S. Madhukar, A. V. Radhakrishnan, A. K. Majhi, and V. A. Raghunathan, *J. Chem. Phys.* **153**, 224901 (2020).
- [31] O. A. Pyshkina and V. G. Sergeev, *Polym. Sci. Ser. C* **54**, 48 (2012).
- [32] A. J. Steckl, *Nat. Photon.* **1**, 3 (2007).